Applied Geography 100 (2018) 78–89

Contents lists available at ScienceDirect

Applied Geography

journal homepage: www.elsevier.com/locate/apgeog

# Appraisal of the Sentinel-1 & 2 use in a large-scale wildfire assessment: A case study from Portugal's fires of 2017

Alexander R. Brown[a], George P. Petropoulos[b,*], Konstantinos P. Ferentinos[c]

[a] Department of Geography and Earth Sciences, University of Aberystwyth, SY23 3DB, Wales, United Kingdom
[b] Department of Soil & Water Resources, Institute of Industrial & Forage Crops, Hellenic Agricultural Organization "Demeter", Larissa, Greece
[c] Department of Agricultural Engineering, Institute of Soil & Water Resources, Hellenic Agricultural Organization "Demeter", Athens, Greece

ARTICLE INFO

*Keywords:*
Sentinel-1
Sentinel-2
Burnt area mapping
Burn severity
RUSLE
Soil erodibility
Support vector machines
Maximum likelihood
Agriculture
Forestry
Earth observation
GIS

ABSTRACT

The recent launch of Sentinel missions offers a unique opportunity to assess the impacts of wildfires at higher spatial and spectral resolution provided by those Earth Observing (EO) systems. Herein, an assessment of the Sentinel-1 & 2 to map burnt areas has been conducted. Initially the use of Sentinel-2 solely was explored, and then in combination with Sentinel-1 and derived radiometric indices. As a case study, the large wildfire occurred in Pedrógão Grande, Portugal in 2017 was used. Burnt area estimates from the European Forest Fires Information System (EFFIS) were used as reference. Burnt area was delineated using the Maximum Likelihood (ML) and Support Vector Machines (SVMs) classifiers, and two multi-index methods. Following this, burn severity was assessed using SVMs and Artificial Neural Networks (ANNs), again for both standalone Sentinel-2 data and in combination with Sentinel-1 and spectral indices. Soil erosion predictions were evaluated using the Revised Universal Soil Loss Equation (RUSLE) model. The effect of the land cover derived from CORINE operational product was also evaluated across the burnt area and severity maps. SVMs produced the most accurate burnt area map, resulting a 94.8% overall accuracy and a Kappa coefficient of 0.90. SVMs also achieved the highest accuracy in burn severity levels estimation, with an overall accuracy of 77.9% and a kappa of 0.710. From an algorithmic perspective, implementation of the techniques applied herein, is based on EO imagery analysis provided nowadays globally at no cost. It is also robust and adaptable, being potentially integrated with other high EO data available. All in all, our study contributes to the understanding of Mediterranean landscape dynamics and corroborates the usefulness of Sentinels data in wildfire studies.

## 1. Introduction

Wildfires pose a significant threat to both environment and infrastructure across the globe (Colson, Petropoulos, & Ferentinos, 2018; Kalivas, Petropoulos, Athanasiou, & Kollias, 2013). They constitute an important area of study due to the plethora of effects that can have on people and the environment. There are three main components that form the optimal conditions required for a fire to take place: low moisture levels, dry windy weather, and a fire material for combustion (Ireland & Petropoulos, 2015; Running, 2006). As a result of the frequent occurrence of these optimal conditions for fire outbreaks in the Mediterranean (Inbar, Lado, Sternberg, Tenau, & Ben-Hur, 2014), there is a high rate of wildfires within this region. In recent years, the size of wildfires has increased with large-scale fire events contributing a higher percentage towards total area burnt (Ganteaume & Jappiot, 2013; Kalivas et al., 2013; Said, Petropoulos, & Srivastava, 2015).

The use of Earth Observation (EO) allows for an efficient and cost-effective analysis of fire events. This is due to the fact that the user can obtain information from the chosen study site without visiting that particular area (Lamine et al., 2017; Roy, Boschetti, & Smith, 2013). Predicting wildfire occurrence is difficult. Hence it can be challenging to obtain pre-fire observations through field-based methods. EO in this case can provide useful pre-fire information as satellite systems consistently monitor the same areas periodically (Morgan et al., 2014; Evans et al., in press). Classifications performed in recent years have tended to move away from the original methods and algorithms for classifying an image, which generally gave more emphasis to probability distributions, e.g. the maximum likelihood or parallelepiped classifiers. Instead, non-parametric approaches have been favored, which include algorithms such as random forests. These non-parametric

* Corresponding author. Department of Soil & Water Resources, Institute of Industrial & Forage Crops, Hellenic Agricultural Organization "Demeter", Larissa, Greece.
*E-mail address:* petropoulos.george@gmail.com (G.P. Petropoulos).

https://doi.org/10.1016/j.apgeog.2018.10.004
Received 16 May 2018; Received in revised form 5 August 2018; Accepted 15 October 2018
Available online 22 October 2018
0143-6228/ 

approaches allow the user to investigate non-linear relationships within the data. Despite the usefulness of those approaches, implementation of such classifiers are not always necessary (Huang et al., 2016).

New remote sensing systems such as those onboard the Sentinel-1 & 2 platforms, allow data acquisition at higher spectral and spatial resolutions in comparison to previously available open-access information (Chatziantoniou, Petropoulos, & Psomiadis, 2017; Drusch et al., 2012; Markogianni, Kalivas, Petropoulos, & Dimitriou, 2018; Vhengani et al., 2015; Whyte, Fredinos, & Petropoulos, 2018). Huang et al. (2016) noted that due to the nature of the Sentinel-2 sensor, with multiple bands that are useful for examining vegetation, it might be the case that there is correlation between the bands. A number of wildfire studies, performed both inside and outside of the Mediterranean, have used multiple classifiers to assess the accuracy and validate the data that the researcher has obtained (Colson et al., 2018; Oertel, Lorenz, & Halle, 2010; Petropoulos, Kontoes, & Keramitsoglou, 2012, 2010; Stroppiana et al., 2015; Zhang et al., 2017).

Portugal is one of the most fire-prone countries in Southern Europe. Local and national government promoted the timber industries during the twentieth century, leading to an increased availability of fuel to forest fires (Moreira, Rego, & Ferreira, 2001). Oliveira, Pereira, and Carreiras (2012) used the Weibull function to estimate that approximately 1.2% of the country was burnt annually. It was found that fires in this region were covering a significantly larger area as a percentage of the country when compared to other countries such as Greece or Spain, meaning that significantly more people are likely to be affected by fires in Portugal. However, despite its history with fires, significantly less research surrounds Portugal's wildfires when compared to other Mediterranean countries, with significantly fewer studies conducted within the country.

On an annual basis, fire coverage in Portugal ranges from 15,462 hectares to 440,000 hectares (Oliveira et al., 2012). Thus, the selected case study, the recent large-scale wildfire event that occurred in the Pedrógão Grande region and the surrounding areas, with an estimated burnt area of 70,000 hectares, is of particularly high significance, as the burnt area of that single event is much greater than those of some entire fire seasons (Jones, 2017a; Marques et al., 2011; Oliveira et al., 2012). Even though the European Forest Fire Information System (EFFIS) estimated the burnt area to be 46,769 hectares, it is still considered to be a significant large-scale wildfire event (EFFIS, 2017).

In this study, an assessment of Sentinel-1 & 2 data to provide accurate wildfire related products is made. Key objective is to accurately map and assess the impacts of the recent large wildfire that occurred in the surrounding areas of Pedrógão Grande, Portugal, in June 2017. The usefulness of Sentinel data in particular is assessed, with specific goals to: i) produce burnt area maps through multiple approaches and compare their accuracies, ii) create burn severity maps to highlight the most affected areas, iii) assess the post-fire soil erosion, and iv) analyze the effect of the land cover to the fire behavior using land cover data from CORINE (Coordination of Information on the Environment) operational product.

## 2. Materials and methods

### 2.1. Study site

Pedrógão Grande is located in central Portugal within the Leiria district (Fig. 1-A). With a population of approximately 4000 people, it represents quite a remote rural community. One of the main industries in the area is the wood industry, which represents a significant portion of the local economy (INE, 2014; Moreira et al., 2001). This site was chosen due to the proximity of the event and the reported large-scale devastation that the fire caused to the areas surrounding Pedrógão Grande, therefore making it an interesting case study. The area of interest, which comprises approximately a quarter of a Sentinel-2 scene, covers a region of approximately 167,521 hectares. A breakdown of land cover types that are present in the area, according to the CORINE land cover (CLC) database, is shown in Fig. 1-B, with the corresponding quantitative data included in Table 1. The dominance of forested areas in the region is evident, with more than 83% of the study area comprising of forests and semi-natural areas. Fig. 1 also shows the pre-fire (sub-figure C) and post-fire (sub-figure D) conditions across the study area, based on Sentinel-2 images. The beginning of the wildfire was reported to occur due to a lightning strike that was located close to the small town of Escalos Fundeiros (Jones, 2017b), which is also shown in Fig. 1-C and 1-D.

### 2.2. Datasets and pre-processing

Between other investigators, Malenovský et al. (2012) explored the potential of the Sentinel sensors for use in scientific studies, suggesting synergistic approaches that make use of more than one sensor type. One area in which they highlighted for the use of this type of approach was within burnt area studies. Sentinel-1 operates a synthetic aperture radar working at C-band frequency (5.405 GHz), first launched in 2014. The sensor has multiple data collection modes enabling a number of products to be obtained. As part of a two-satellite system, Sentinel-1A and Sentinel-1B, delivering products with a six-day return period at the equator, offering users a range of products specific to individual needs. The products are available as two data types: Ground Range Detected (GRD) and Single Look Complex (SLC) (Geudtner, Torres, Snoeij, Davidson, & Rommen, 2014; Moreira et al., 2013). For this study, Interferometric Wide Swath GRD was chosen. This product is available at a 5 m × 20 m resolution at a 250 km swath. The selected scene was collected on July 7, 2017, following the date that the fire event had been reported to have been extinguished. The specific scene was also chosen as it was the closest to that of the corresponding Sentinel-2 scene.

Sentinel-2 also operates as part of a two-satellite system, and it provides high resolution multispectral optical imagery. Two optical images were sourced to provide data for this study. They were selected as they were the closest imagery available around the ignition and suppression dates. Fortunately, the imagery was cloud-free across the study area in both scenes, so there was no data loss from needing to cloud masks the imagery. The pre-fire image was captured on June 16, and the post-fire image on July 4, 2017 (Fig. 1C and D).

Sen2Cor is a third party tool produced in partnership with the European Space Agency (ESA) that applies atmospheric corrections to achieve the bottom of atmosphere (BOA) surface reflectance for Sentinel-2 Level 1C products, producing a Level 2A product ready for analysis. It was used in this study as it has been previously implemented in studies that make use of Sentinel-2 imagery and also within studies that explore wildfires (Chatziantoniou et al., 2017; Hirschmugl, Deutscher, Gutjahr, Sobe, & Schardt, 2017; Huang et al., 2016; Navarro et al., 2017; Notarnicola et al., 2017; Novelli, Aguilar, Nemmaoui, Aguilar, & Tarantino, 2016; Whyte et al., 2018). Following the application of Sen2Cor, the files were exported as a GeoTIFF to allow for manipulation in other software packages. To align with the SAR dataset that is being used to supplement the optical data, the outputs were resampled to 20 m resolution to allow for stacking the bands together later in the process. Following this, the scene was subset to the study area. Fig. 1-C and -D show the outputs following the pre-processing of the scene subset to the study area.

The acquired Sentinel-1 data needed to be pre-processed to provide a reliable backscatter (dB) value. All of the pre-processing steps were performed within SNAP 5.0. The orbital file was initially applied to correct for any orbital errors that may have occurred. Following this, radiometric calibration was conducted to convert the values to sigma nought. A terrain correction was also applied; here SNAP sources 30 m SRTM data. As is common in SAR data, there was considerable speckle within the scene. Even though this is not “noise”, it is undesirable due to the nature of the contrasts that occur across a scene (Lillesand,

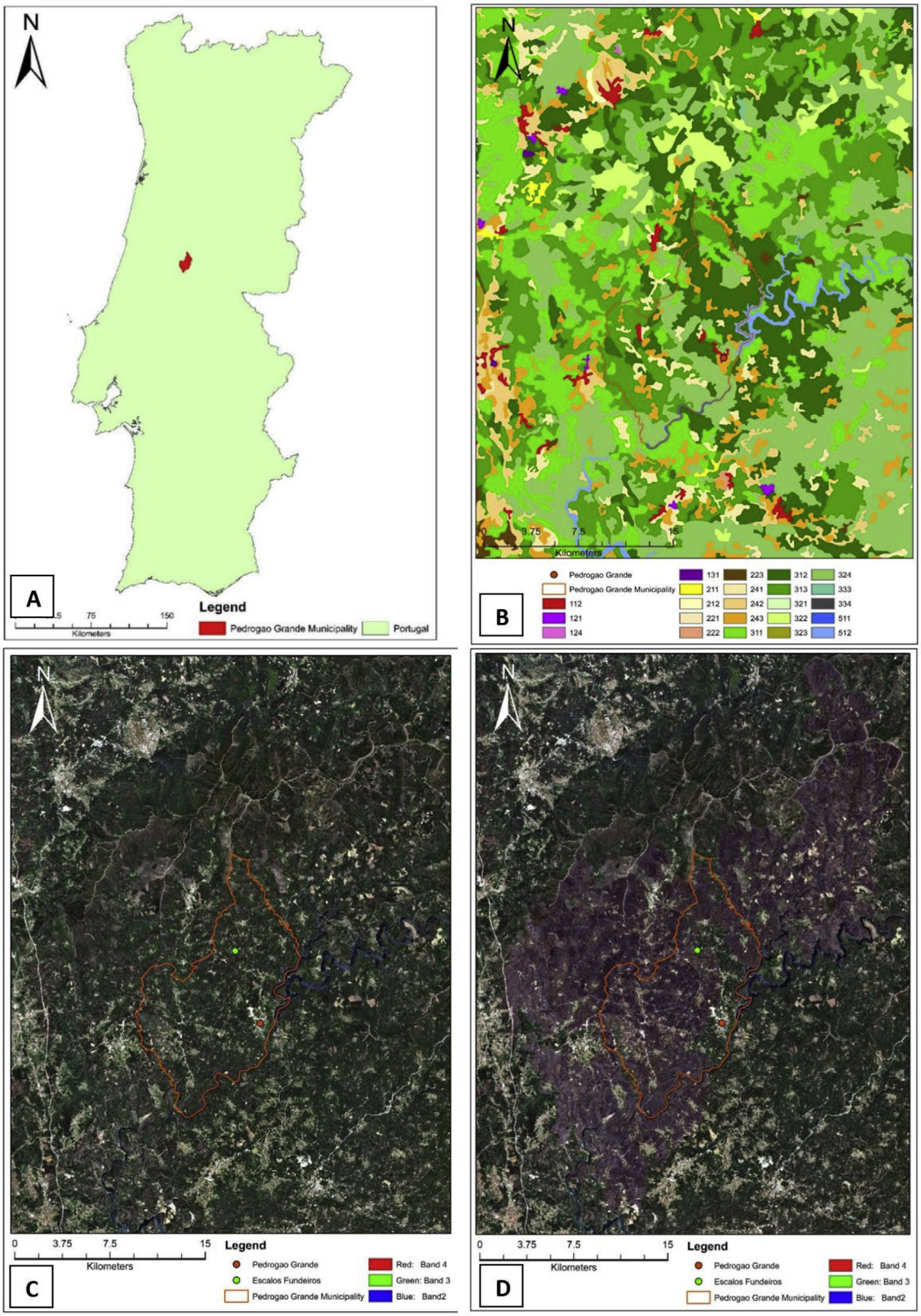


**Fig. 1.** Location of the area of interest (municipality of Pedrógão Grande, Portugal) (A), its land cover types (B) (reference numbers are explained in Table 1), and Sentinel-2 pre-fire (C) and post-fire (D) conditions in RGB – true color composite. (For interpretation of the references to color in this figure legend, the reader is referred to the Web version of this article.)

**Table 1**
Distribution of land cover types across the study area.

| CLC type | Nomenclature | Area (ha) | % of total land cover |
|---|---|---|---|
| 112 | Discontinuous Urban | 1647.12 | 0.98 |
| 121 | Industrial or Commercial | 239.96 | 0.14 |
| 124 | Airports | 26.52 | 0.02 |
| 131 | Mineral Extraction Sites | 64.68 | 0.04 |
| 211 | Non-Irrigated Arable Land | 547.12 | 0.33 |
| 212 | Permanently Irrigated Land | 192.04 | 0.11 |
| 221 | Vineyards | 163.32 | 0.10 |
| 222 | Fruit trees and berry plantations | 126.92 | 0.08 |
| 223 | Olive Groves | 978.88 | 0.58 |
| 241 | Annual Crops | 5675.72 | 3.39 |
| 242 | Complex Cultivations | 7236.32 | 4.32 |
| 243 | Principally Agriculture with Significant Natural Vegetation | 8392.84 | 5.01 |
| 311 | Broad-Leaved Forest | 25479.6 | 15.21 |
| 312 | Coniferous Forest | 27257.08 | 16.27 |
| 313 | Mixed Forest | 33522.84 | 20.01 |
| 321 | Natural Grassland | 36.16 | 0.02 |
| 322 | Moors and Heathland | 5061.12 | 3.02 |
| 323 | Sclerophyllous Vegetation | 259.16 | 0.15 |
| 324 | Transitional Woodland/Shrub | 48540.64 | 28.98 |
| 333 | Sparsely Vegetated Areas | 72.36 | 0.04 |
| 334 | Burnt Areas | 53.68 | 0.03 |
| 511 | Inland Waters | 198.36 | 0.12 |
| 512 | Marine Waters | 1748.76 | 1.04 |
| | TOTAL | 167521.20 | 100.00 |

Kiefer, & Chipman, 2015). Therefore the “Refined Lee” filter was applied to reduce speckle, as this is commonly used due to its high performance (Foucher & López-Martínez, 2009; Lavreniuk et al., 2017). Finally, the backscatter values were converted to decibels. Following this, the scene was exported as a GeoTIFF, resampled to 20 m to align with the Sentinel-2 data and then subset to the study area extent. The files produced after completion of this pre-processing step were used to implement the main processing to satisfy the study objectives.

### 2.3. Processing and analysis

Table 2 outlines the specific products used in our study. Following identification of prominent indices used for burnt area mapping and discriminating burn severity levels, multiple indices were calculated. Table 3 outlines the indices included within this study and their corresponding calculation formulas based on the Sentinel-2 bands. This processing was undertaken within QGIS with the raster calculator tool. The indices were created with the aim of stacking with the Sentinel data before the classifications were performed. They also proved a useful tool for examining the burn across the study area.

**Table 2**
Methods used for each task and corresponding data (indices are analyzed in Table 3).

| Product | Method | Data |
|---|---|---|
| Burnt area | | |
| 1 | Maximum Likelihood | Optical |
| 2 | Maximum Likelihood | Optical, Radar |
| 3 | Maximum Likelihood | Optical, Radar, Indices |
| 4 | Support Vector Machines | Optical, Radar, Indices |
| 5 | Multi-index 1 | NBR, NDVI, gNDVI |
| 6 | Multi-index 2 | Clre, NDre1, NDre2, MSRre, MSRren |
| Burn severity | | |
| 1 | Support Vector Machines | Optical, Radar, Indices |
| 2 | Artificial Neural Networks | Optical, Radar, Indices |
| Soil erosion | | |
| 1 | Model | RUSLE |
| Fire analysis | | |
| 1 | Burnt area statistics | CORINE |
| 2 | Burn severity statistics | CORINE |

**Table 3**
Spectral indices used, and their corresponding formulas based on Sentinel-2 bands.

| Abbreviation | Spectral Index | Band formula |
|---|---|---|
| Clre | Chlorophyll Red Edge | (B7/B5)-1 |
| NDre1 | Normalised Difference Red Edge 1 | (B6-B5)/(B6 + B5) |
| NDre2 | Normalised Difference Red Edge 2 | (B7-B5)/(B7 + B5) |
| MSRre | Modified Simple Ratio Red Edge | ((B8/B5)-1)/sqrt((B8/B5) + 1) |
| MSRren | Modified Simple Ratio Red Edge Narrow | ((B8a/B5)-1)/sqrt((B8a/B5) + 1) |
| NBR | Normalised Burn Ratio | (B8-B12)/(B8 + B12) |
| NDVI | Normalised Difference Vegetation | (B8-B4)/(B8 + B4) |
| gNDVI | Green Normalised Difference Vegetation | (B8-B3)/(B8 + B3) |

**Table 4**
Prepared stacked bands, used for classification.

| Stack band | Input data | Stack band | Input data |
|---|---|---|---|
| 1 | Sentinel-2 Band 2 | 10 | Sentinel-2 Band 12 |
| 2 | Sentinel-2 Band 3 | 11 | VV (db) |
| 3 | Sentinel-2 Band 4 | 12 | VH (db) |
| 4 | Sentinel-2 Band 5 | 13 | Clre |
| 5 | Sentinel-2 Band 6 | 14 | NDre1 |
| 6 | Sentinel-2 Band 7 | 15 | NDre2 |
| 7 | Sentinel-2 Band 8 | 16 | MSRre |
| 8 | Sentinel-2 Band 8a | 17 | MSRren |
| 9 | Sentinel-2 Band 11 | | |

Subsequently, it was necessary to stack the obtained bands in order to perform the classifications within the ENVI software (5.0). This involved the creation of three new image stacks, one including solely the Sentinel-2 bands of 20 m resolution, the second with the optical stacked with the SAR bands, and the third including also some of the calculated indices. Table 4 presents the bands used. Three GeoTIFF's were created, the first with bands 1–10, the second with bands 1–12 and the third including all bands, 1–17. These specific indices are particularly useful in determining burnt areas (Fernández-Manso, Fernández-Manso, & Quintano, 2016).

#### 2.3.1. Burnt area mapping

To perform the required burnt area mapping, a number of classifications were performed. Maximum Likelihood (ML) and Support Vector Machine (SVMs) classifiers have been extensively used previously in relevant context (e.g., Chen, Moriya, Sakai, Koyama, & Cao, 2016; Foody, 2015; Liu et al., 2016; Petropoulos, Vadrevu, Xanthopoulos, Karantounias, & Scholze, 2010; Petropoulos et al., 2012; Sertel & Alganci, 2016). In order to perform the classifications, training data was required to train the classifiers. In total 50,000 pixels were used for training for each of the two classes, burnt area and unburnt areas. A random sampling scheme was used for the collection of these pixels. Subsequently, the ML classifier was initially applied to the optical image, and then the two additional stacked images (the first including SAR bands and the second including other indices, as shown in Table 4). Next, the SVMs classifier was used upon the combined data set (optical, SAR and indices). A linear kernel was chosen due to the low number of classes required, as only determination of burnt and unburnt areas was sought. Parametrization of the SVMs was based on suggestions from the literature (Elatawneh, Kalaitzidis, Petropoulos, & Schneider, 2014; Petropoulos, Kontoes, & Keramitsoglou, 2011).

Because there is still uncertainty as to which indices are the best for determining burnt areas, an effective combination of indices was

considered as an appropriate approach. Two multi-index methods were used within this study. The first, Multi-index 1, comprises of the NBR, NDVI and gNDVI, as these are used widely across a range of sensors to determine burnt areas. The second, Multi-index 2, uses newer indices, making use of the additional spectral bands available to Sentinel-2, which are capable of distinguishing between burn severity levels and therefore useful to discriminate between burnt and unburnt areas. Multi-index 2 comprises of: Clre, NDre1, NDre2, MSRre and MSRren. Due to their nature, indices do not provide a binary, burnt or unburnt areas as the classifiers are able to produce. The OTSU threshold was applied to separate burnt from unburnt areas (Otsu, 1979). This was chosen as it has been successfully used in wildfire studies, and is able to produce the binary output that is desired to outline the burnt areas (Vala & Baxi, 2013; Vhengani et al., 2015).

#### 2.3.2. Burn severity mapping

Two classifiers were chosen to distinguish burn severity levels, Artificial Neural Networks (ANNs) and SVMs. Both have been used previously in wildfire studies with a high degree of accuracy and are widely known to perform well (Kavzoglu & Mather, 2003; Petropoulos et al., 2010; Srivastava, Han, Rico-Ramirez, Bray, & Islam, 2012; Ul-Islam, Abbas, Ahmad, Shah, & Saeed, 2017; Wan-Kadir, Latiff, Rasib, & Rahman, 2012, pp. 1–6). In order to reduce the chances of misclassification from the original images, especially surrounding the lower burn severity levels, the burnt area map with the highest performing accuracy assessment was used to mask out the rest of the scene before performing the classification. A burn perimeter was created to further mask out any outlying misclassified pixels. The classifications were again performed within ENVI 5.0, which allows for parameterization of the classifiers. When performing the SVMs classification, multiple runs were performed with the aim of identifying optimal parameters. The polynomial kernel was chosen for the burn severity mapping. For the ANNs, the parameters were chosen as best identified from the literature. A one hidden-layer network architecture was selected, as has been favored in similar studies, and based on the fact that one hidden-layer ANNs are universal approximators, meaning that they can approximate any nonlinear function (Fine, 2006). Other network training parameters were selected based on a combination of previous implementations found within the literature and appropriate experimentation. As a result, the training threshold contributor was set to 0.9, the training rate to 0.15, the training momentum to 0.9 and the maximum training iterations to 1500.

#### 2.3.3. Soil erodibility mapping

To implement the soil erosion model, the five components comprising the Revised Universal Soil Loss Equation (RUSLE) model need to be estimated: R – rainfall erosivity, K – soil erodibility, LS – topographic slope/slope length, C – vegetation cover factor, and P – agri-practice support. The LS factor is heavily influenced by the terrain of the area. The DEM used to calculate the LS factor was obtained from the USGS Earth Explorer platform, with a resolution of 30 × 30 meters. Then, as in Magesh and Chandrasekar (2016), it was necessary to obtain a number of products from the DEM for input into the LS function. This function is determined by the slope, and in this case, a power of 0.4 was used as a result of the topography present in the area. The K factor was obtained from the European Soil Data Centre (ESDAC). The R, P and C factors were also obtained from ESDAC, which were available at 500 m, 1 km, and 100 m resolutions, respectively. The burn severity outputs were used to determine the C factor score. Moderately damaged received a value of 0.55, as recommended in the literature (Karamesouti, Petropoulos, Papanikolaou, Kairis, & Kosmas, 2016). This was altered to 0.50 for slightly damaged, 0.60 for highly damaged and 0.65 for completely destroyed. This alteration was performed in order to distinguish between severity levels within the burnt area, as areas more affected by fire are likely to have reduced vegetation cover. Once all factors were derived, RUSLE was implemented, with output an indicator of soil erosion across the area of interest.

#### 2.3.4. Accuracy assessment and fire analysis

Accuracy assessment is a common place in land cover classifications, forming the standard method for validating generated output maps (Foody, 2002). ArcMap 10.5 was used for that purpose. The kappa coefficient is also commonly used in classification assessments, as it provides an overview from a statistical basis. Kappa values range from 0 to 1, where 0.5 determines that the classification was no better than random, and higher values representing better classifications (De Leeuw et al., 2006). Each burnt area map was assessed using 1000 points per class, and burn severity maps were assessed using 400 points per class The points were selected using a random sampling scheme, and in such a way to cover all the spectral variability within each class, variability resulting from differences for example due to vegetation health condition, vegetation properties such as fractional cover of vegetation, soil moisture content etc.

To give additional context to the wildfire event, affected land cover types were sought with the aim of determining which land cover type was most affected following the fire, which may possibly give an insight into some of the economic, environmental and social costs that occurred during this large scale wildfire. In order to achieve this, CORINE operational product was consulted, provided by the Copernicus Land Monitoring Service. The most accurate burnt area map was used to extract the land cover information. This processing was also conducted within ArcMap 10.5. Land cover was assessed for both the burnt area and then an assessment was made to the levels of severity that each land cover type observed. To remove some of the 'speckle' errors that are commonly associated with pixel based approaches within the burnt area estimation, a majority filter was applied. This reduced the total burnt area that was derived from the SVMs classifier from 40,279.70 ha to 39,624.2 ha, representing a 655.50 ha change in estimation. The CORINE data was clipped to the filtered burnt area raster.

## 3. Results

### 3.1. Burnt area mapping

The maps delineating the burnt areas are shown in Fig. 2, while the corresponding total burnt areas and estimation accuracies are provided in Table 5. The burnt area map with the highest accuracy comprised of the SVMs classification of all of the available data, using the Sentinel-1, Sentinel-2 and calculated index bands. This provided an estimated affected area of 40,279.7 ha. Among the compared methods, the first multi-index performed the worst, with both multi-index methods performing significantly lower than the other methods. Generally, each method performed well in displaying the "core" burnt areas, but the multi-index methods included significantly more "speckle" or areas in which single pixels were distributed across the study area. When comparing the multi-index methods with the original imagery, it becomes clear that this method performed not so well in areas surrounding the river. While the multi-index methods did achieve total burnt area values that were closer to the reference Rapid Damage Assessment (RDA) fire values, the other methods achieved higher classification scores. The multi-index methods greatly over-estimated burnt area, as it can be observed by the accuracy assessment findings (Table 6). Accuracy assessment was performed through the use of the 10 m outputs of the Sentinel imagery and assessment against the reference dataset. This method was followed as there are no high resolution Emergency Management Service maps yet, that could be considered as "truth". In addition to this, no in-situ "field" data was available. The same number of points were used to conduct the accuracy assessment of each classification, i.e. ~1000 points per class. The results presented in Table 6 make clear that, while the SVMs more accurately represented the unburnt areas, the ML accurately presented more burnt area points. Both of the Multi-index methods performed

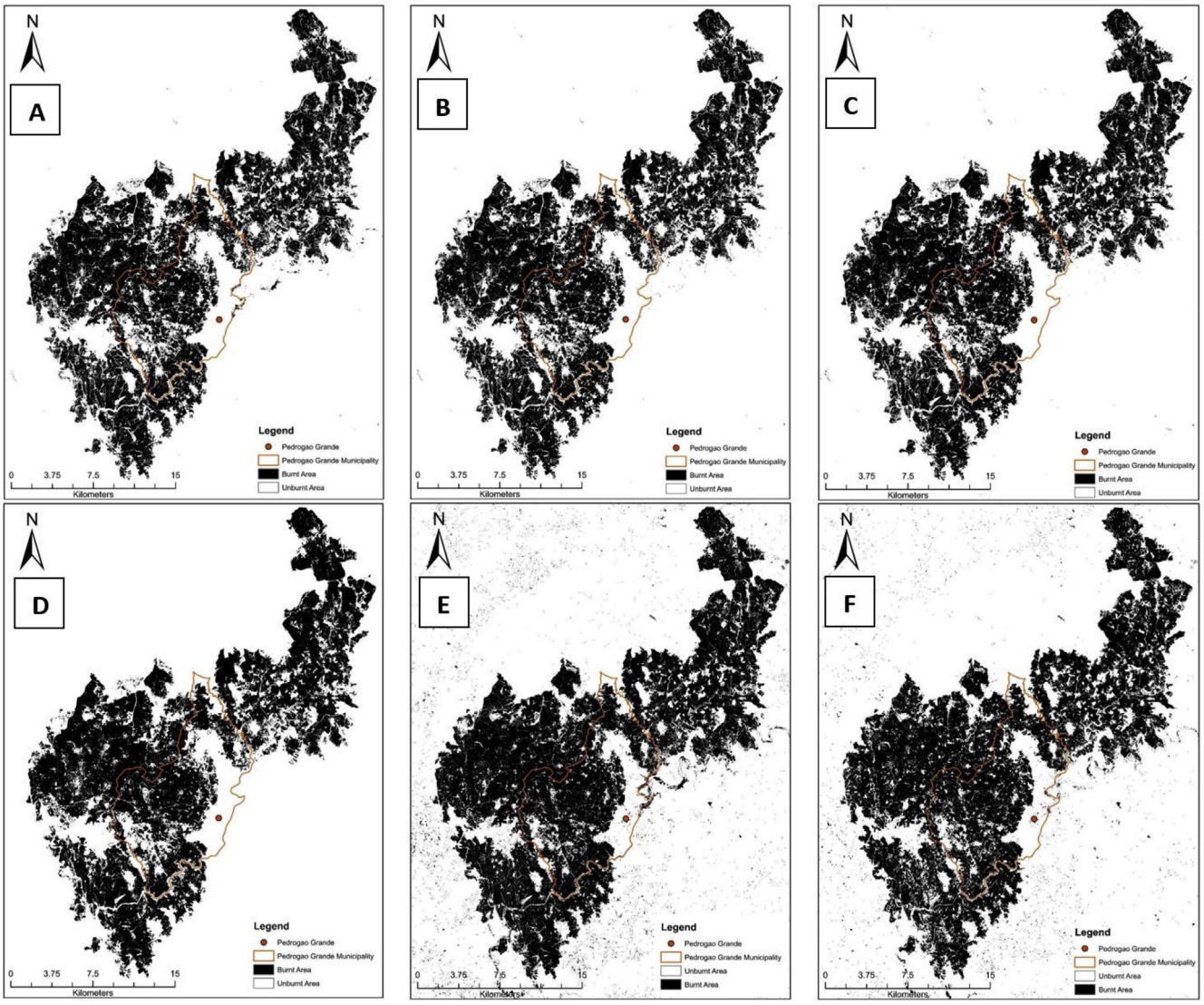


**Fig. 2.** Burnt area mapping classifications using, A: ML with stack bands 1–10, B: ML with stack bands 1–12, C: ML with stack bands 1–17, D: SVMs with stack bands 1–17, E: Multi-index 1, F: Multi-index 2.

**Table 5**
Total burnt areas and estimation accuracies for each classification method.

| Method | Burnt area (Ha) | Classification accuracy (%) | Kappa coefficient |
|---|---|---|---|
| Maximum Likelihood (O) | 33,603.4 | 90.5 | 0.81 |
| Maximum Likelihood (O + R) | 33,698.8 | 91.1 | 0.82 |
| Maximum Likelihood (O + R + I) | 34,959.4 | 94.6 | 0.89 |
| Support Vector Machines | 40,279.7 | 94.8 | 0.90 |
| Multi-index 1 | 42,441.4 | 82.8 | 0.66 |
| Multi-index 2 | 38,790.6 | 84.2 | 0.68 |
| EFFIS estimate | 46,769.0 | n/a | n/a |

somewhat poorly, with both methods providing low correct identification of burnt and unburnt with significant points misclassified.

### 3.2. Burn severity assessment

Burn severity was assessed using the datasets presented in Table 2. The outcome is shown in Fig. 3, based on both SVMs and ANNs, while Table 7 presents a comparison of the given areas by the two classifiers. From visual inspection of the imagery it can be observed that both classifiers broadly determined the same areas as the same level of severity. It can also be seen that the highest differences in the severity assessment between the two methods concerned the moderately damaged and highly damaged classes. Classification accuracies were performed again using the 10 m Sentinel-2 outputs as reference, and their corresponding index calculations. Table 8 shows the distribution of points across the error matrix for the burn severity maps. It can be observed that the SVMs achieved higher classification accuracy, returning 77.9% whereas ANNs achieved 74.5%. The SVMs product also had a significantly higher kappa coefficient, suggesting that this output is more accurate. In both classifications, the completely destroyed and slightly damaged classes obtained much better user accuracies when compared to the highly damaged and moderately damaged classes.

### 3.3. Soil erosion model

A pre-fire and post-fire model was developed to demonstrate the implications of the fire for soil erosion. The RUSLE model was applied, as described in sub-section 2.3.3. Fig. 4-A shows the pre-fire soil loss

**Table 6**
Accuracy assessment error matrices for the burnt area maps (method numbers 1–6 are better defined in Table 2).

| 1. ML-O | Burnt | Unburnt | Total | User (%) | 4. SVM | Burnt | Unburnt | Total | User (%) |
|---|---|---|---|---|---|---|---|---|---|
| Burnt | 902 | 98 | 1000 | 90.2 | Burnt | 931 | 69 | 1000 | 93.1 |
| Unburnt | 92 | 908 | 1000 | 90.8 | Unburnt | 35 | 965 | 1000 | 96.5 |
| Total | 994 | 1006 | 2000 | | Total | 966 | 1034 | 2000 | |
| Producer (%) | 90.7 | 90.3 | | | Producer (%) | 96.4 | 93.3 | | |
| Accuracy (%) | 90.5 | | | | Accuracy (%) | 94.8 | | | |
| Kappa coeff. | 0.81 | | | | Kappa coeff. | 0.90 | | | |
| **2. ML-O + R** | **Burnt** | **Unburnt** | **Total** | **User (%)** | **5.Multi-ind.1** | **Burnt** | **Unburnt** | **Total** | **User (%)** |
| Burnt | 912 | 88 | 1000 | 91.2 | Burnt | 791 | 209 | 1000 | 79.1 |
| Unburnt | 90 | 910 | 1000 | 91.0 | Unburnt | 135 | 865 | 1000 | 86.5 |
| Total | 1002 | 998 | 2000 | | Total | 926 | 1074 | 2000 | |
| Producer (%) | 91.0 | 91.2 | | | Producer (%) | 85.4 | 80.5 | | |
| Accuracy (%) | 91.1 | | | | Accuracy (%) | 82.8 | | | |
| Kappa coeff. | 0.82 | | | | Kappa coeff. | 0.66 | | | |
| **3. ML-O + R + I** | **Burnt** | **Unburnt** | **Total** | **User (%)** | **6.Multi-ind.2** | **Burnt** | **Unburnt** | **Total** | **User (%)** |
| Burnt | 950 | 50 | 1000 | 95.0 | Burnt | 809 | 191 | 1000 | 80.9 |
| Unburnt | 58 | 942 | 1000 | 94.2 | Unburnt | 126 | 874 | 1000 | 87.4 |
| Total | 1008 | 992 | 2000 | | Total | 935 | 1065 | 2000 | |
| Producer (%) | 94.2 | 95.0 | | | Producer (%) | 86.5 | 82.1 | | |
| Accuracy (%) | 94.6 | | | | Accuracy (%) | 84.2 | | | |
| Kappa coeff. | 0.89 | | | | Kappa coeff. | 0.68 | | | |

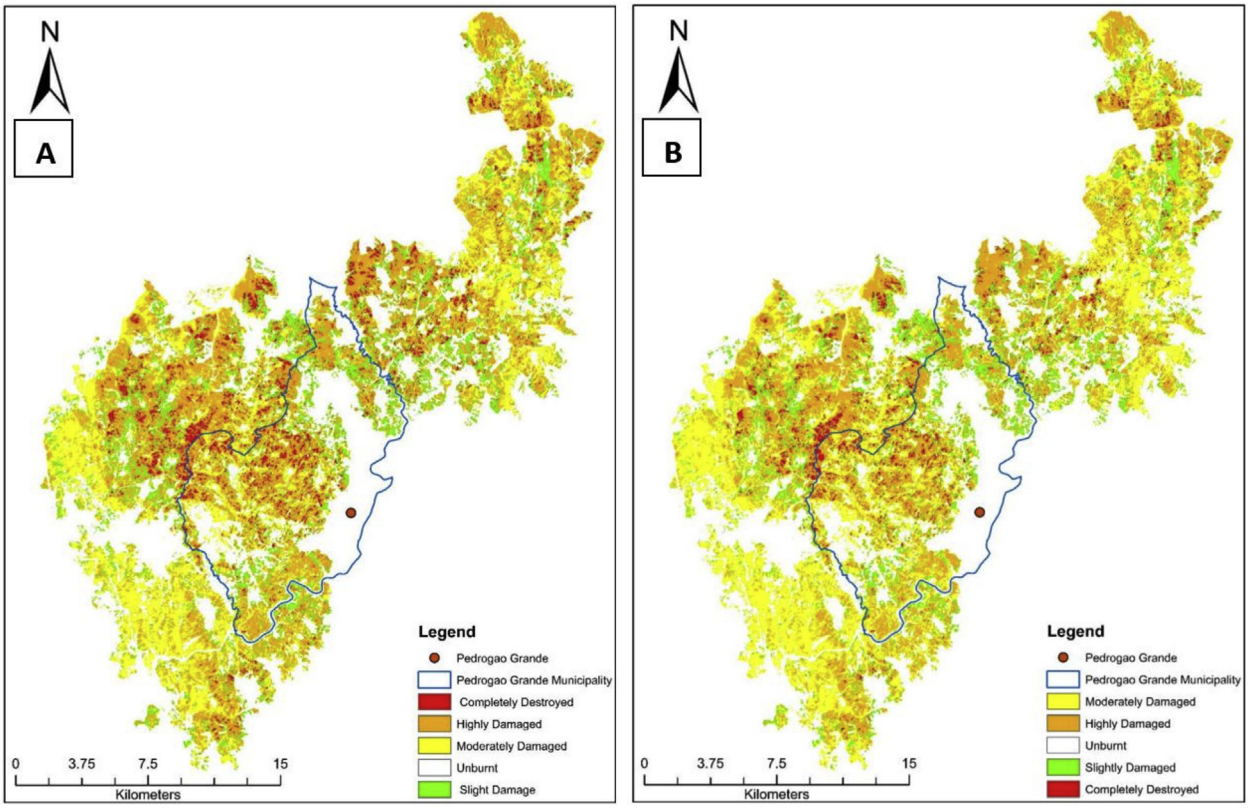


**Fig. 3.** Burn severity map classified by SVMs (A) and ANNs (B).

conditions. Predominantly, the erosion factor is low across the study area with a few isolated moderate risk factors and very few areas which reach towards the top of the erosion scale. The erosion is displayed in tons per hectare per year, where categories were separated by the natural breaks within the data. Fig. 4-B presents the soil erosion conditions following the fire. It can be observed that there is a widespread change across the study area. Areas that are labeled as “moderate erosion” increased towards the higher scale of erosion. There are also significant areas across the study area that progress up the erosion scale from the lowest erosion rate.

### 3.4. Analysis of effects on land cover types

Fig. 5 shows the CORINE land cover classification across the burnt area delineation, using the SVM methodology. Following extraction of the land cover type to the affected burnt area, statistics were calculated

**Table 7**
Burn severity areas estimated by SVMs and ANNs.

| Severity level | SVMs (Ha) | ANNs (Ha) | Estimation difference (Ha) |
|---|---|---|---|
| Completely Destroyed | 2269.8 | 1405.9 | 863.9 |
| Highly Damaged | 16,267.8 | 13,396.5 | 2871.3 |
| Moderately Damaged | 10,966.6 | 14,919.9 | 3953.3 |
| Slightly Damaged | 6303.6 | 5647.5 | 656.1 |
| Total | 35,807.8 | 35,369.8 | 438.0 |

**Table 8**
Error matrices for burn severity maps (number of points), where, CD: Completely Destroyed, HD: Highly Damaged, MD: Moderately Damaged, SD: Slightly Damaged.

| **SVMs** | **CD** | **HD** | **MD** | **SD** | **Total** | **User (%)** |
|---|---|---|---|---|---|---|
| CD | 362 | 1 | 30 | 7 | 400 | 90.5 |
| HD | 19 | 274 | 76 | 31 | 400 | 68.5 |
| MD | 22 | 67 | 269 | 42 | 400 | 67.3 |
| SD | 6 | 9 | 43 | 342 | 400 | 85.5 |
| Total | 409 | 351 | 418 | 422 | 1600 | |
| Producer (%) | 88.5 | 78.1 | 64.4 | 81.0 | | |
| **Overall accuracy (%)** | **77.9** | | | | | |
| **Kappa coefficient** | **0.71** | | | | | |

| **ANNs** | **CD** | **HD** | **MD** | **SD** | **Total** | **User (%)** |
|---|---|---|---|---|---|---|
| CD | 346 | 21 | 23 | 10 | 400 | 86.5 |
| HD | 29 | 254 | 89 | 28 | 400 | 63.5 |
| MD | 25 | 64 | 272 | 39 | 400 | 68.0 |
| SD | 7 | 20 | 53 | 320 | 400 | 80.0 |
| Total | 407 | 359 | 437 | 397 | 1600 | |
| Producer (%) | 85.0 | 70.8 | 62.2 | 80.6 | | |
| **Overall accuracy (%)** | **74.5** | | | | | |
| **Kappa coefficient** | **0.66** | | | | | |

for these areas. This was performed to present an indication of the affected land cover types, and thus to provide an insight into some of the main effects of the wildfire event. The same data is presented quantitatively in Table 9. CLC 313 (Mixed Forest) had the greatest affected area. There are multiple land cover classes that were affected minimally, of these some were not vegetation based classes, such as 121, 511 and 512, likely as a result of misclassification within the burnt area map and the spatial resolution of the CLC product. The main affected areas were all forest based. Table 9 also shows the percentage of the burnt area for each class in terms of the total area of each class within the study area.

Table 10 offers an inter-comparison of the ANNs and SVMs delineation of burn severity across the present land cover types. From these values, it is evident that some classes were comparatively small, covering less than ten hectares, as a result of the breakdown of the affected burnt area presented in Table 9. The SVMs generally classified a greater proportion of the affected area as completely destroyed, highly damaged and slightly damaged, across all classes, with the ANNs presenting a greater area as moderately damaged across CLC types.

## 4. Discussion

The burnt area outputs provided by the classifications performed within this study show that the Sentinel-2 platform can provide an accurate tool for mapping burnt areas. The addition of the Sentinel-1 SAR bands did not show to have a significant impact upon the classification; at least this was the case in this particular study. The latter suggests that a synergistic approach may not necessarily yield more accurate results in assessing burnt areas for regions similar to the one under investigation here. ML and SVMs performed significantly better than the multi-index methods, which had significant speckle within the scene. Following the implementation of a majority filter upon the index-based methods, speckle was significantly reduced, thus this

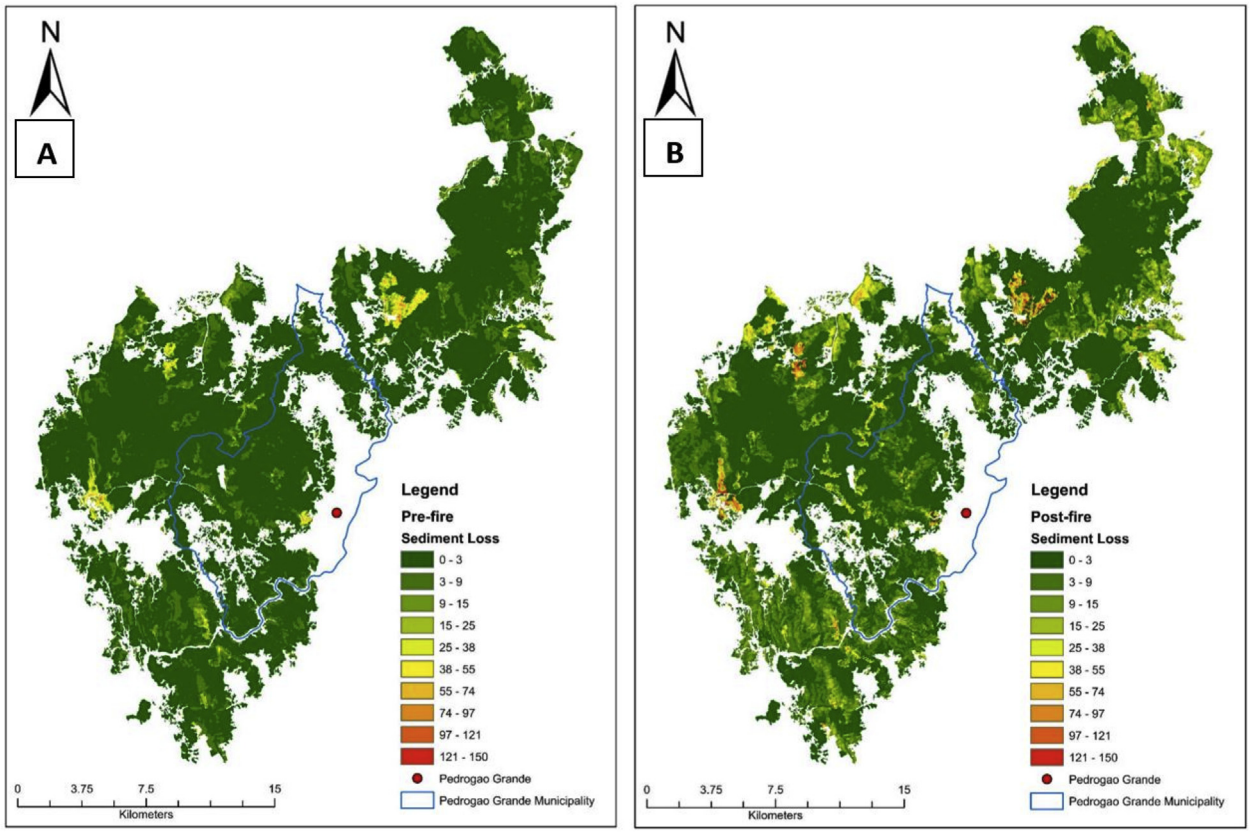


**Fig. 4.** RULSE model pre-fire (A) and post-fire (B) conditions, in tons per hectare per year.

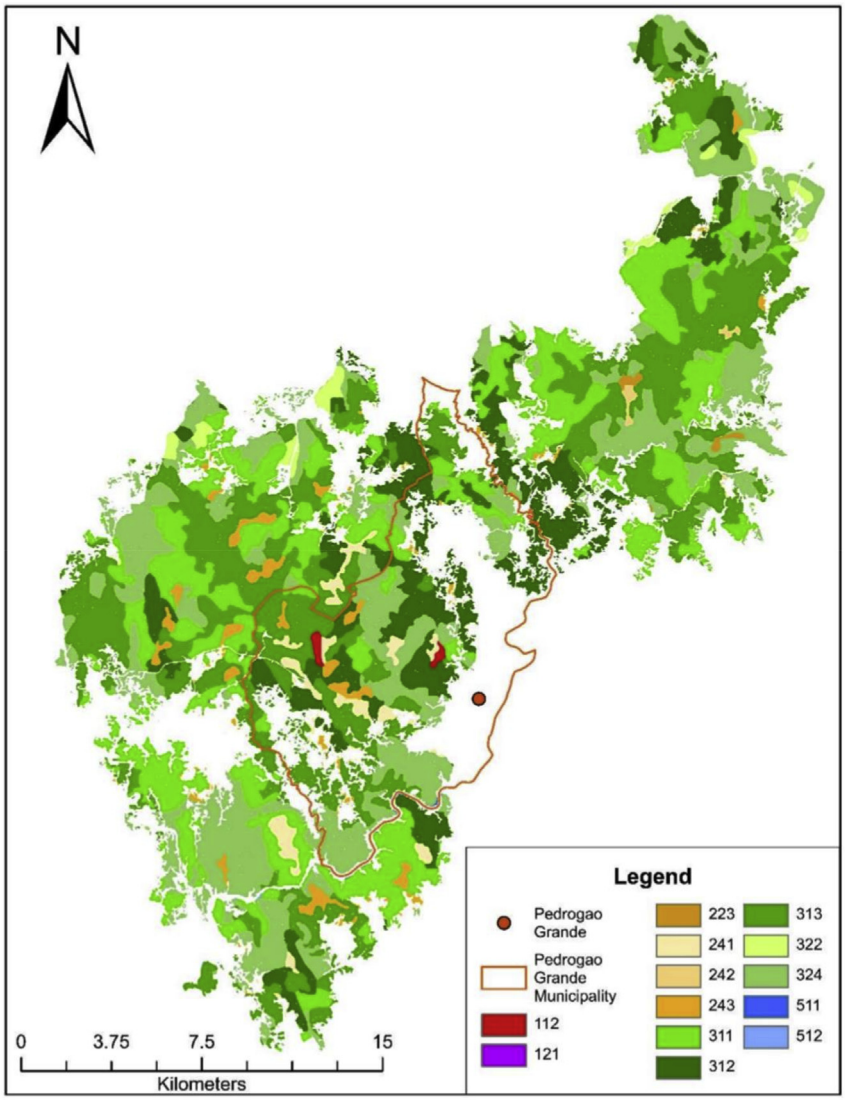


**Fig. 5.** The extracted CORINE land cover map across the burnt area. CLC classes are defined in Tables 1 and 9.

**Table 9**
CORINE land cover across the burnt area, as displayed in Fig. 5.

| CLC | Nomenclature | Area (Ha) | Percentage of Total Burn (%) | Percentage of Study Area CLC (%) |
|---|---|---|---|---|
| 112 | Discontinuous Urban | 80.2 | 0.2 | 4.9 |
| 121 | Industrial or Commercial | 1.1 | 0.003 | 0.5 |
| 223 | Olive Groves | 79.2 | 0.2 | 8.1 |
| 241 | Annual Crops | 772.6 | 1.9 | 13.6 |
| 242 | Complex Cultivations | 89.6 | 0.2 | 1.2 |
| 243 | Agriculture with Significant Vegetation | 956.04 | 2.4 | 11.4 |
| 311 | Broad-Leaved Forest | 9664.4 | 24.4 | 37.9 |
| 312 | Coniferous Forest | 5678.4 | 14.3 | 20.8 |
| 313 | Mixed Forest | 11,572.9 | 29.2 | 34.5 |
| 322 | Moors and Heathland | 516.0 | 1.3 | 10.2 |
| 324 | Transitional Woodland/Shrub | 10,196.8 | 25.7 | 21.0 |
| 511 | Inland Waters | 7.72 | 0.02 | 3.4 |
| 512 | Marine Waters | 9.16 | 0.02 | 0.5 |
| | Total | 39,624.2 | 100.0 | |

approach could help to improve the delineation of the burnt area. This method could be useful to investigators who are solely interested in the location of the fire event and in a broad examination of the fire, as the application of the filter makes clearer the location of the main burnt areas. The benefit of using the multi-index method compared to the other classification methods was that these were significantly quicker to implement, enabling a rapid assessment of the fire, which could be of particular interest to those who are working within a time critical environment.

It can also be observed that the RDA provided by the EFFIS significantly overestimated the extent of the fire. It may be the case that this was due to the resolution of the sensors that were being used and the fact that the shapefile provided by EFFIS generalized the outline of the fire. This suggests that studies that use these estimations for analyzing the trends of burnt areas across time may misrepresent the actual extent of the burnt area. Overall, the classification performed well, and this was aided by the fact that there was no cloud within the study area. Finally, it can be observed that the use of a stacked image making use of spectral indices offered an improvement to the classification.

The two burn severity outputs show that there was widespread devastation, with significant areas witnessing moderate damage or above. There was a degree of variance between the two outputs in terms of the areas determined as high to moderately damaged. This somewhat

**Table 10**
Burn severity statistics per land cover type across the burnt area (in hectares). CD: Completely Destroyed, HD: Highly Damaged, MD: Moderately Damaged, and SD: Slightly Damaged.

| CLC | CD | | HD | | MD | | SD | |
|---|---|---|---|---|---|---|---|---|
| | ANNs | SVMs | ANNs | SVMs | ANNs | SVMs | ANNs | SVMs |
| 112 | 0.08 | 0.12 | 0.80 | 2.16 | 16.88 | 15.28 | 2.68 | 2.96 |
| 121 | 0.00 | 0.00 | 0.24 | 0.28 | 0.60 | 0.60 | 0.00 | 0.04 |
| 223 | 0.00 | 0.00 | 3.48 | 6.28 | 17.24 | 13.72 | 3.80 | 4.76 |
| 241 | 2.24 | 3.08 | 38.56 | 72.04 | 326.00 | 293.68 | 32.16 | 43.56 |
| 242 | 0.76 | 1.00 | 6.36 | 8.92 | 22.84 | 20.20 | 3.20 | 4.04 |
| 243 | 7.56 | 9.04 | 93.12 | 170.32 | 407.84 | 325.80 | 107.08 | 131.76 |
| 311 | 297.28 | 538.08 | 3372.88 | 4045.52 | 3672.76 | 2590.76 | 1392.28 | 1647.92 |
| 312 | 296.16 | 489.12 | 2009.40 | 2389.68 | 1496.04 | 999.76 | 1463.56 | 1447.72 |
| 313 | 554.48 | 813.88 | 3962.04 | 4880.28 | 4156.16 | 2923.28 | 1801.92 | 1978.36 |
| 322 | 2.28 | 3.72 | 247.16 | 254.64 | 244.88 | 246.88 | 5.96 | 4.64 |
| 324 | 244.80 | 410.92 | 3660.60 | 4434.16 | 4554.72 | 3535.12 | 828.32 | 1028.84 |
| 511 | 0.12 | 0.24 | 0.56 | 1.24 | 2.84 | 1.16 | 2.32 | 3.68 |
| 512 | 0.16 | 0.60 | 1.28 | 2.32 | 1.08 | 0.32 | 4.24 | 5.32 |
| Total | 1405.9 | 2269.8 | 13396.5 | 16267.8 | 14919.9 | 10966.6 | 5647.5 | 6303.6 |

highlights the difficulty in determining differences between severity levels, particularly without ground truth information. The two outputs performed broadly the same in terms of the areas that they portrayed as completely destroyed and areas of slight damage, suggesting that these severity levels are easier to discern. This could prove useful to those attempting to determine the most affected areas following a fire, assisting in the implementation of post-fire recovery strategies as response teams are likely to prioritize those areas that were damaged the most. SVMs was deemed to be more accurate than the ANNs, suggesting that this method is more appropriate for this type of applications, given the level of training that was provided to the classifiers. Computationally, SVMs was also faster than the ANNs, which took significantly longer to process. The severity maps can also assist in quantifying the damage caused by the fire. When compared to the land cover types, an assessment of the destruction within individual land cover types can be made. The burn severity product can be used as an output to inform decision makers, or can be used to inform models and extract useful information.

A rule-based classifier could help to improve the burn severity accuracies presented in the results section, particularly for the severity outputs. Using an accurate burnt area delineation as a mask to remove classification errors, a set of rules could be determined based on the indices outlined as useful for determining burn severity (Fernández-Manso et al., 2016). This could provide a more robust separation of burn severity. The inclusion of fewer classes could also help improve the classification, as for example, the implementation of low, medium and high severity (Quintano, Fernández-Manso, & Roberts, 2013). Nevertheless, the outputs provided within this study distinguish severity to a reasonable accuracy across the four classes, especially for completely destroyed and slightly damaged areas. Both classifiers struggled with the middle severity values, potentially due to the similarity between these classes.

Following the fire, there is likely to be significant additional soil erosion, as can be observed from the contrast between the two images of Fig. 4. The post-fire product presents a map that could be useful to decision makers seeking to implement prevention measures to reduce soil erosion. It provides an indication as where to best implement strategies such as the construction of soil erosion barriers, mulching and seeding (Colson et al., 2018; Fernández & Vega, 2016; Vega, Fernández, & Fonturbel, 2015). Despite the use of the post-fire severity map to inform the vegetation cover factor, this represents only one fifth of the model parameters, so may not necessarily adequately help to represent significant change between the pre- and post-fire models. However, significant change could still be observed between the scenes despite this. The model could be improved by the addition of finer resolution datasets. As datasets were obtained from the ESDAC, which provides European wide datasets, the resolutions of some of these data types were fairly coarse. Overall, the RUSLE model provided a useful indication of potential soil erosion following the fire.

From the fire analysis results, it can be seen that, predominantly, forested areas were affected by this fire event. The smallest area, industrial, made up only a hectare of the affected area, totaling less than 0.01% of the entire scene and just 0.46% of the total industrial land cover available in the whole scene. The findings presented in the results section, depicting significant forest damage, highlight the devastating social and economic effects that wildfires can have in Portugal, especially in this region. With the wood industry making up a large portion of the economy in this region, the economic and social impacts of this fire, given that significant forested areas were burnt, would be severe. A main drawback of the CORINE assessment approach is the fact that the level of land ownership cannot be determined. While it can discriminate between affected land cover types, it cannot interpret directly whether these forests are used for commercial purposes or whether they are naturally occurring forests. However, it can be assumed that significant forest cover in this region is used for commercial purposes.

The use of EO data brings significant benefits when compared to extensive field based studies, particularly given the current level of open access imagery as costs to assess the same area can be significantly reduced. Finally, the output maps presented within this study provide accurate and useful products. Solely using EO data does have its limitations. It can be difficult to distinguish severity levels with complete certainty without adequate ground truth information. However, this study chose to use only publicly available data.

## 5. Conclusions

A recent large-scale wildfire surrounding the town of Pedrógão Grande was assessed, and the usefulness of Sentinel data for assessing wildfire events was explored. It has been demonstrated that the SVMs classifier performs well when compared to other classification methods, providing both the most accurate burnt area estimation and severity map outputs. This study has explored the ability of the combined Sentinel products to improve classification accuracies. Using additional SAR bands only slightly improved output maps whereas, combining these with derived indices that have been identified as effective assessors of burnt areas, produced significantly better results. A classification accuracy of 94.8% was achieved for the SVMs burnt area map and 77.9% for the SVMs severity map. These accuracies support the use of Sentinel data for wildfire assessment.

This study performed solely pixel-based classifications, which returned high levels of accuracy. A soil erosion model has also been presented, to demonstrate the influence of the wildfire event upon

erosion across the study area. Land cover has also been assessed, highlighting the significant level of damage that occurred as a result of this wildfire event. Forested areas contributed to a significant portion of the burnt area. Hence, potential economic and long-term consequences may be significant. Almost 70% of the area affected by the fire was directly classed as forest (Mixed, Coniferous or Broad-leaved) according to CORINE, plus an additional 25% represented as transitional woodland/shrub. This highlights the severe damage that has been caused to the local economy of Pedrógão Grande, as much of this area relies upon the wood industries. Given the effectiveness of the methods used in this study, there is potential for the Sentinel platforms to accurately assess burnt areas. While the combination of Sentinel-1 and Sentinel-2 data did not provide significant improvements, at least in this particular study, combination of these data types could prove useful in other areas, but this is subject to further investigations. From an algorithmic perspective, implementation of the techniques implemented herein is based on satellite imagery analysis provided nowadays globally at no cost. It is also easy and computationally inexpensive to be applied, robust and adaptable towards the investigation of other geographical regions and potentially adjustable to be potentially integrated with other high EO data available.

## Author contributions

ARB conducted the research described in this study under the supervision and guidance of GPP, and KPF and GPP wrote the manuscript and also did the manuscript revision.

## Acknowledgments

GPP's contribution to this work was supported by NERC's Newton Fund RCUK project Towards a Fire Early Warning System for Indonesia (ToFEWSI) and the FP7-People project ENViSIon-EO (project reference number 752094). The author wishes to thank the funding bodies for the financial support provided.

## Appendix A. Supplementary data

Supplementary data to this article can be found online at https://doi.org/10.1016/j.apgeog.2018.10.004.

## References

Chatziantoniou, A., Petropoulos, G. P., & Psomiadis, E. (2017). Co-orbital sentinel 1 and 2 for LULC mapping with emphasis on wetlands in a mediterranean setting based on machine learning. *Remote Sensing, 9*. https://doi.org/10.1080/10106049.2017.130746 1-1.

Chen, W., Moriya, K., Sakai, T., Koyama, L., & Cao, C. X. (2016). Mapping a burned forest area from Landsat TM data by multiple methods. *Geomatics, Natural Hazards and Risk, 7*(1), 384–402.

Colson, D., Petropoulos, G. P., & Ferentinos, K. P. (2018). Exploring the potential of Sentinels-1 & 2 of the Copernicus mission in support of rapid and cost-effective wildfire assessment. *International Journal of Applied Earth Observation & Geoinformation, 73*, 262–276.

De Leeuw, J., Jia, H., Yang, L., Liu, X., Schmidt, K., & Skidmore, A. K. (2006). Comparing accuracy assessments to infer superiority of image classification methods. *International Journal of Remote Sensing, 27*(1), 223–232.

Drusch, M., Del Bello, U., Carlier, S., Colin, O., Fernandez, V., Gascon, F., et al. (2012). Sentinel-2: ESA's optical high-resolution mission for GMES operational services. *Remote Sensing of Environment, 120*, 25–36.

EFFIS (2017). *Copernicus emergency management Service.* European Commission. 25 July, [Online]. Available at: http://effis.jrc.ec.europa.eu/static/effis_current_situation/public/index.html, Accessed date: 25 July 2017.

Elatawneh, A., Kalaitzidis, C., Petropoulos, G. P., & Schneider, T. (2014). Evaluation of diverse classification approaches for land use/cover mapping in a Mediterranean region utilizing Hyperion data. *International Journal of Digital Earth, 7*(3), 194–216.

Evans, A., Lamine, S., Kalivas, D., & Petropoulos, G. P. (2014). *Exploring the potential of EO data and GIS for ecosystem health modelling in response to wildfire: A case study in Central Greece.* Environmental Engineering & Management (in press).

Fernández-Manso, A., Fernández-Manso, O., & Quintano, C. (2016). SENTINEL-2A red-edge spectral indices suitability for discriminating burn severity. *International Journal of Applied Earth Observation and Geoinformation, 50*(1), 170–175.

Fernández, C., & Vega, J. A. (2016). Are erosion barriers and straw mulching effective for controlling soil erosion after a high severity wildfire in NW Spain? *Ecological Engineering, 87*(1), 132–138.

Fine, T. L. (2006). *Feedforward neural network methodology*. Springer Science Business Media.

Foody, G. M. (2002). Status of land cover classification accuracy assessment. *Remote Sensing of Environment, 80*(1), 185–201.

Foody, G. M. (2015). The effect of mis-labeled training data on the accuracy of supervised image classification by SVM. *Geoscience and remote sensing symposium, July, IGARSS* (pp. 4987–4990). IEEE International.

Foucher, S., & López-Martínez, C. (2009). An evaluation of PolSAR speckle filters. *Geoscience and remote sensing symposium, July IEEE international: Vol. 4*, (pp. 1–4). IGARSS.

Ganteaume, A., & Jappiot, M. (2013). What causes large fires in Southern France. *Forest Ecology and Management, 294*, 76–85.

Geudtner, D., Torres, R., Snoeij, P., Davidson, M., & Rommen, B. (2014). Sentinel-1 system capabilities and applications. *Geoscience and remote sensing symposium, IGARSS* (pp. 1457–1460). IEEE International.

Hirschmugl, M., Deutscher, J., Gutjahr, K. H., Sobe, C., & Schardt, M. (2017). Combined use of SAR and optical time series data for near real-time forest disturbance mapping. *9th international workshop on the analysis of multitemporal remote sensing images, June* (pp. 1–4). IEEE.

Huang, H., Roy, D. P., Boschetti, L., Zhang, H. K., Yan, L., Kumar, S. S., et al. (2016). Separability analysis of sentinel-2A multi-spectral instrument (MSI) data for burned area discrimination. *Remote Sensing, 8*(10), 873–891.

Inbar, A., Lado, M., Sternberg, M., Tenau, H., & Ben-Hur, M. (2014). Forest fire effects on soil chemical and physicochemical properties, infiltration, runoff, and erosion in a semiarid Mediterranean region. *Geoderma, 221*, 131–138.

INE (2014). *Statistical Information, Pedrógão Grande.* Instituto Nacional De Estatistica. [Online]. Available at: https://www.ine.pt/xportal/xmain?xpid=INE&xpgid=ine_unid_territorial&menuBOUI=13707095& contexto=ut&selTab=tab3, Accessed date: 6 July 2017.

Ireland, G., & Petropoulos, G. P. (2015). Exploring the relationships between post-fire vegetation regeneration dynamics, topography and burn severity: A case study from the montane cordillera ecozones of western Canada. *Applied Geography, 56*, 232–248. https://doi.org/10.1016/j.apgeog.2014.11.016.

Jones, S. (2017a). *Portugal forest fires under control after more than 60 deaths.* The Guardian, 22 June, [Onine]. Available at: https://www.theguardian.com/world/2017/jun/22/portugal-forest- fires-under-control, Accessed date: 25 July 2017.

Jones, S. (2017b). *Portuguese wildfires: Early warnings hindered by damaged phone lines.* The Guardian, 19 June, [Online]. Available at: https://www.theguardian.com/world/2017/jun/19/portuguese-wildfires-water-dropping-planes- spain-france-italy, Accessed date: 25 July 2017.

Kalivas, D. P., Petropoulos, G. P., Athanasiou, I. M., & Kollias, V. J. (2013). An inter-comparison of burnt area estimates derived from key operational products: The Greek wildland fires of 2005–2007. *Nonlinear Processes in Geophysics, 20*(3), 397–409.

Karamesouti, M., Petropoulos, G. P., Papanikolaou, I. D., Kairis, O., & Kosmas, K. (2016). Erosion rate predictions from PESERA and RUSLE at a Mediterranean site before and after a wildfire: Comparison and implications. *Geoderma, 261*(1), 44–58.

Kavzoglu, T., & Mather, P. M. (2003). The use of backpropagating artificial neural networks in land cover classification. *International Journal of Remote Sensing, 24*(23), 4907–4938.

Lamine, S., Petropoulos, G. P., Singh, S. K., Szabo, s., Bachari, N., srivastava, P. K., et al. (2017). Quantifying land use/land cover spatio-temporal landscape pattern dynamics from Hyperion using SVMs classifier and FRAGSTATS. *Geocarto International*. https://doi.org/10.1080/10106049.2017.1307460 (in press).

Lavreniuk, M., Kussul, N., Meretsky, M., Lukin, V., Abramov, S., & Rubel, O. (2017). Impact of SAR data filtering on crop classification accuracy. *First Ukraine conference on electrical and computer engineering* (pp. 1–5). .

Lillesand, T., Kiefer, R. W., & Chipman, J. (2015). *Remote sensing and image interpretation* (7th ed.). New Jersey: Wiley.

Liu, W., Wang, L., Zhou, Y., Wang, S., Zhu, J., & Wang, F. (2016). A comparison of forest fire burned area indices based on HJ satellite data. *Natural Hazards, 81*(2), 971–980.

Magesh, N. S., & Chandrasekar, N. (2016). Assessment of soil erosion and sediment yield in the Tamiraparani sub-basin, South India, using an automated RUSLE-SY model. *Environmental Earth Sciences, 75*(1208), 1–17.

Malenovský, Z., Rott, H., Cihlar, J., Schaepman, M. E., García-Santos, G., Fernandes, R., et al. (2012). Sentinels for science: Potential of Sentinel-1,-2, and-3 missions for scientific observations of ocean, cryosphere, and land. *Remote Sensing of Environment, 120*(1), 91–101.

Markogianni, V., Kalivas, D., Petropoulos, G. P., & Dimitriou, E. (2018). An appraisal of the potential of landsat 8 in estimating chlorophyll-a, ammonium concentrations and other water quality indicators. *Remote Sensing MDPI, 10*, 1–22.

Marques, S., Borges, J. G., Garcia-Gonzalo, J., Moreira, F., Carreiras, J. M. B., Oliveira, M. M., et al. (2011). Characterization of wildfires in Portugal. *European Journal of Forest Research, 130*(5), 775–784.

Moreira, A., Prats-Iraola, P., Younis, M., Krieger, G., Hajnsek, I., & Papathanassiou, K. P. (2013). A tutorial on synthetic aperture radar. *IEEE Geoscience and Remote Sensing Magazine, 1*(1), 6–43.

Moreira, F., Rego, F. C., & Ferreira, P. G. (2001). Temporal (1958–1995) pattern of change in a cultural landscape of northwestern Portugal: Implications for fire occurrence. *Landscape Ecology, 16*(6), 557–567.

Morgan, P., Keane, R. E., Dillon, G. K., Jain, T. B., Hudak, A. T., Karau, E. C., et al. (2014). Challenges of assessing fire and burn severity using field measures, remote sensing and modelling. *International Journal of Wildland Fire, 23*(8), 1045–1060.

Navarro, G., Caballero, I., Silva, G., Parra, P. C., Vázquez, Á., & Caldeira, R. (2017).

Evaluation of forest fire on Madeira Island using Sentinel-2A MSI imagery. *International Journal of Applied Earth Observation and Geoinformation, 58*(1), 97–106.
Notarnicola, C., Asam, S., Jacob, A., Marin, C., Rossi, M., & Stendardi, L. (2017). Mountain crop monitoring with multitemporal Sentinel-1 and Sentinel-2 imagery. *9th international workshop on the analysis of multitemporal remote sensing images, June* (pp. 1–4). IEEE.
Novelli, A., Aguilar, M. A., Nemmaoui, A., Aguilar, F. J., & Tarantino, E. (2016). Performance evaluation of object based greenhouse detection from sentinel-2 MSI and landsat 8 OLI data: A case study from almería (Spain). *International Journal of Applied Earth Observation and Geoinformation, 52*(1), 403–411.
Oertel, D., Lorenz, E., & Halle, W. (2010). *Detection and monitoring of wildfires by a constellation of small satellites with infrared sensor systems.* Copenhagen: Geoinformation for Disaster and Risk Management: Examples and Best Practices.
Oliveira, S. L., Pereira, J. M., & Carreiras, J. M. (2012). Fire frequency analysis in Portugal (1975–2005), using Landsat-based burnt area maps. *International Journal of Wildland Fire, 21*(1), 48–60.
Otsu, N. (1979). A threshold selection method from gray-level histograms. *IEEE Transactions on System, Man & Cybernetics, 9*(1), 62–66.
Petropoulos, G. P., Kontoes, C., & Keramitsoglou, I. (2011). Burnt area delineation from a uni- temporal perspective based on Landsat TM imagery classification using support vector machines. *International Journal of Applied Earth Observation and Geoinformation, 13*(1), 70–80.
Petropoulos, G. P., Kontoes, C. C., & Keramitsoglou, I. (2012). Land cover mapping with emphasis to burnt area delineation using co-orbital ALI and Landsat TM imagery. *International Journal of Applied Earth Observation and Geoinformation, 18*(1), 344–355.
Petropoulos, G. P., Vadrevu, K. P., Xanthopoulos, G., Karantounias, G., & Scholze, M. (2010). A comparison of spectral angle mapper and artificial neural network classifiers combined with Landsat TM imagery analysis for obtaining burnt area mapping. *Sensors, 10*(3), 1967–1985.
Quintano, C., Fernández-Manso, A., & Roberts, D. A. (2013). Multiple endmember spectral mixture analysis (MESMA) to map burn severity levels from landsat images in mediterranean countries. *Remote Sensing of Environment, 136*, 76–88.
Roy, D. P., Boschetti, L., & Smith, A. (2013). Satellite remote sensing of fires. In C. M. Belcher (Ed.). *Fire phenomena and the Earth system: An interdisciplinary guide to fire science* (pp. 77–93). .
Running, S. W. (2006). Is global warming causing more, larger wildfires? *Science, 313*(5789), 927–928.
Said, Y. A., Petropoulos, G. P., & Srivastava, P. K. (2015). Assessing the influence of atmospheric and topographic correction on burnt scars identification from high resolution. *Natural Hazards*. https://doi.org/10.1007/s11069-015-1792-9.
Sertel, E., & Alganci, U. (2016). Comparison of pixel and object-based classification for burned area mapping using SPOT-6 images. *Geomatics, Natural Hazards and Risk, 7*(4), 1198–1206.
Srivastava, P. K., Han, D., Rico-Ramirez, M. A., Bray, M., & Islam, T. (2012). Selection of classification techniques for land use/land cover change investigation. *Advances in Space Research, 50*(9), 1250–1265.
Stroppiana, D., Azar, R., Calò, F., Pepe, A., Imperatore, P., Boschetti, M., et al. (2015). Integration of optical and SAR data for burned area mapping in Mediterranean Regions. *Remote Sensing, 7*(2), 1320–1345.
Ul-Islam, S., Abbas, A. W., Ahmad, A., Shah, S., & Saeed, K. (2017). Parameter investigation of artificial neural network and support vector machine for image classification. *14th international bhurban conference on applied sciences and technology (IBCAST), January* (pp. 795–798). IEEE.
Vala, M. H. J., & Baxi, A. (2013). A review on Otsu image segmentation algorithm. *International Journal of Advanced Research in Computer Engineering and Technology (IJARCET), 25*(10), 1231–1240.
Vega, J. A., Fernández, C., & Fonturbel, T. (2015). Comparing the effectiveness of seeding and mulching + seeding in reducing soil erosion after a high severity fire in Galicia (NW Spain). *Ecological Engineering, 74*(1), 206–212.
Vhengani, L., Frost, P., Lai, C., Booi, N., van den Dool, R., & Raath, W. (2015). Multitemporal burnt area mapping using Landsat 8: Merging multiple burnt area indices to highlight burnt areas. *International geoscience and remote sensing symposium, July, IGARSS* (pp. 4153–4156). IEEE.
Wan-Kadir, W. H., Latiff, S. Z. A., Rasib, A. W., & Rahman, M. Z. A. (2012). *Increasing accuracy of image classification using artificial neural network.* Malaysia: Department of Geoinformation, Faculty of Geoinformation and Real Estate1–6. http://a-a-r-s.org/acrs/administrator/components/com_jresearch/files/publications/SC02-0723_INCREASING-ACCURACY-OF-IMAGE-CLASSIFICATION-USING-ARTIFICIAL-NEURAL-NETWORK.pdf, Accessed date: 19 August 2017.
Whyte, A., Fredinos, K., & Petropoulos, G. P. (2018). A new synergistic approach for monitoring wetlands using Sentinels -1 and 2 data with object-based machine learning algorithms. *Environmental Modelling & Software, 104*, 40–57.
Zhang, T., Su, J., Liu, C., Chen, W. H., Liu, H., & Liu, G. (2017). Band selection in sentinel-2 satellite for agriculture applications. *Proceedings of the 23rd international conference on automation and computing* (pp. 1–6). .